



# Oxidative carbonylation of methane to acetic acid over micro-mesoporous rhodium-modified zeolites

Natalia V. Kolesnichenko, Yulia M. Sntenkova, Tatiana I. Batova\*, Olga V. Yashina, Konstantin B. Golubev

A.V. Topchiev Institute of Petrochemical Synthesis, Russian Academy of Sciences, Prospect 29, Leninsky, Moscow, 119991, Russia

## ARTICLE INFO

### Keywords:

Methane  
Acetic acid  
Rhodium  
Micro-mesoporous ZSM-5 zeolites

## ABSTRACT

It was first demonstrated that under liquid-phase conditions, an increase in the mesoporosity of ZSM-5 zeolite boosts a rhodium-containing catalyst activity in the oxidative carbonylation of methane to acetic acid (the acetic acid yield is  $570 \mu\text{mol g}_{\text{cat}}^{-1}$ ). To increase the mesoporosity of zeolite, two approaches were used: ultrasonic treatment and desilication of zeolite. The ultrasonic pretreatment leads to an increase in the acetic acid yield with a decrease in the total yield of oxygenates (methanol/acetic acid molar ratio is 0.2). On the contrary, preliminary desilication contributes to an increase in the total yield of oxygenates, mainly due to methanol (methanol/acetic acid molar ratio is 1.8). The combination of ultrasonic pretreatment and desilication of zeolite improves the total yield of oxygenates with an increase in the acetic acid yield. Such a change in the catalytic properties is attributed both to the acidity of the parent zeolite and the local atomic environment of rhodium. XAS spectroscopy showed that rhodium can be present on the zeolite surface either as nanoclusters giving rise to methanol or as isolated rhodium atoms, which promote the acetic acid formation.

## 1. Introduction

The development of environmentally friendly processes for the production of intermediate petrochemicals from carbon-containing raw materials is an urgent, scientific and engineering task. The most common carbonaceous source is methane. The transformation of methane into valuable functionalized products is a major challenge of modern chemistry, and, in particular, the catalytic synthesis of acetic acid (AA) from methane and carbon monoxide is of great interest.

Currently, AA is manufactured by methanol carbonylation. Methanol is synthesized from syngas, which is in turn obtained during the steam reforming of methane or coal at high temperatures. Replacing the existing high-temperature catalysis in the production of AA with catalysis at low temperatures would be possible if the process on a heterogeneous catalyst effectively converted methane directly into AA under mild conditions.

Noble metal-based supported catalysts have not been seriously considered before due to the slight deep dissociation of the C–H bond and the reoxidation of the methane molecule to carbon dioxide on the metal sites. Nevertheless, the one-stage conversion of methane to methanol or AA was carried out on homogeneous Pt- or Pd-based

catalysts, however, using aggressive oxidizing agents or media [1,2]. Besides, theoretical studies have shown that metal sites with a lower value of the coordination number can stabilize  $\text{CH}_3$  species thereby avoiding the subsequent methane dehydrogenation [3]. The use of zeolites as support materials has recently attracted much attention owing to the presence of Brønsted acid sites (BAS) in zeolites. The methane oxidation on zeolites is assumed to occur through the methoxy groups formed on the BAS. Such groups may serve as intermediates in many other types of reactions to obtain industrially important products.

Recently, Flytzani-Stephanopoulos et al. made a great breakthrough by oxidizing methane not only to methanol, but also to AA under mild conditions on a single-atom rhodium-containing ZSM-5 catalyst [4]. Unlike rhodium atoms anchored in non-porous silicates and other oxides, this heterogeneous catalyst exhibits high performance in the conversion of methane to AA. The conversion of methane to methanol and AA on isolated palladium and rhodium atoms fixed in a zeolite framework in a liquid medium has been studying since the beginning of 2012, and it has become one of the fundamental modern approaches for developing catalysts towards high catalytic activity and selectivity [5–8].

Another principal approach to enhance the catalyst efficiency is the

\* Corresponding author.

E-mail address: [batova.ti@ips.ac.ru](mailto:batova.ti@ips.ac.ru) (T.I. Batova).

creation of zeolites with an increased proportion of mesopores, since the main disadvantage of microporous zeolites is their easy deactivation associated with internal diffusion limitations. For bulk or branched molecules, only active sites are accessible near the pore mouths of zeolites or on their external surface, which make up no more than 5% of the total number of active sites [9]. In order to obtain micro-mesoporous zeolites, synthetic and post-synthesizing methods of processing industrial zeolite samples are used, such as ultrasonic treatment (UST) [10], desilication (DS), and dealumination [11]. We have shown that the UST of zeolite not only reduces the zeolite size, but also increases the proportion of mesopores [10]. However, the conventional method of obtaining micro-mesoporous zeolites is DS [12]. DS is an inexpensive, simple and more commercially viable method of modifying the textural properties of industrial zeolites compared to syntheses using expensive templates. For DS of ZSM-5 with a  $\text{SiO}_2/\text{Al}_2\text{O}_3$  molar ratio of 50–100, a sodium hydrate solution is used as a solvent to leach silicon to form mesopores [13].

We have previously demonstrated that on ZSM-5 zeolites of the CBV (Zeolyst Int.) with a different  $\text{SiO}_2/\text{Al}_2\text{O}_3$ , the methane oxidative carbonylation proceeds with the formation of methanol and AA, with the yield of total oxygenates depending on the  $\text{SiO}_2/\text{Al}_2\text{O}_3$  [6]. Introduction of rhodium into zeolite in an amount of 0.1–0.5 wt % significantly increases the AA yield, while it is shown that the methane oxidation reaction runs with the simultaneous catalytic involving the acid sites of the bare zeolite and the sites formed by reactive rhodium species.

Here, we investigated the oxidative carbonylation of methane to AA on micro-mesoporous rhodium-modified ZSM-5 zeolites of the CBV brand with a  $\text{SiO}_2/\text{Al}_2\text{O}_3$  of 80. To increase the mesoporosity of the zeolite, two approaches were used: UST and DS of the zeolite. To assess the effect of the zeolite texture properties in the oxidative conversion of methane to AA, the activity of rhodium catalysts supported on conventional microporous zeolite was performed.

## 2. Experimental

### 2.1. Catalyst preparation

In this work, we used microporous ZSM-5 zeolites of the CBV brand with a  $\text{SiO}_2/\text{Al}_2\text{O}_3$  molar ratio of 80. To obtain the H-form (HZSM-5), a sample of zeolite manufactured in ammonium form was calcined at 500 °C in a muffle furnace for 4 h in air.

Post-synthetic treatment of microporous HZSM-5 was carried out by DS. The parent zeolite was treated with a NaOH solution of different molarity (0.1–0.5 M) and decationized with 1.0 M  $\text{NH}_4\text{NO}_3$ . This procedure leads to replacing alkaline cations that are localized in large cavities with protons thus freeing up the porous space. The zeolites with different  $\text{SiO}_2/\text{Al}_2\text{O}_3$  were previously desilicated with an alkali of various molarity. It was shown that zeolite with  $\text{SiO}_2/\text{Al}_2\text{O}_3$  of 80 is best desilicated at a NaOH solution concentration of 0.5 M. The analysis of the zeolite porous structure depending on  $\text{SiO}_2/\text{Al}_2\text{O}_3$  and NaOH concentration is given in the Supplementary data (Table S1, Fig. S1).

Zeolites were exposed to UST in an Elmasonic P30H (ELMA GmbH & Co. KG) ultrasonic bath (frequency, 80 kHz) for 1 h, the concentration of zeolite in water is 1 wt %. The size of the obtained particles was determined by dynamic light scattering on a Zetasizer NANO SZ (Malvern Instruments Co.) particle analyzer. The average particle size is 570–620 nm [10].

Rhodium-containing zeolites (Rh/HZSM-5) were prepared in various ways:

Sample 1 was derived from microporous HZSM-5 by impregnation. A composite of an aqueous solution of  $\text{RhCl}_3 \times 4\text{H}_2\text{O}$  (JSC “Aurat”) and chitosan hydrochloride (manufactured by LLC “Bioprogress”) with a molecular weight of  $10^4$  Da was added to the zeolite during mixing. The mixture was allowed to

stand for 24 h followed by evaporation, then the samples were dried and calcined at 500 °C for 4 h in air.

Sample 2 was prepared similarly to sample 1, with the only difference that HZSM-5 was pretreated with ultrasound.

Sample 3 was prepared similarly to sample 1, with the only difference that HZSM-5 was pretreated with 0.5 M NaOH solution and decationized with 1 M  $\text{NH}_4\text{NO}_3$ .

Sample 4 was prepared similarly to sample 1, with the only difference that HZSM-5 was pretreated with 0.5 M NaOH solution and decationized with 1 M  $\text{NH}_4\text{NO}_3$  and then treated with ultrasound.

Sample 5 was prepared similarly to sample 1 with the only difference that HZSM-5 was pretreated with ultrasound and then treated with a 0.5 M NaOH solution and decationized with 1 M  $\text{NH}_4\text{NO}_3$ .

The Rh content in the rhodium-containing zeolite catalysts is 0.5 wt %. The elemental composition of the catalysts is given in the Supplementary data (Table S2).

### 2.2. Catalyst characterization

*Textural characteristics* (specific surface area, total pore volume, and pore size distribution) of the samples were studied at a temperature of 77 K by nitrogen low-temperature adsorption/desorption on a Micromeritics ASAP-2010 instrument. All samples were pre-evacuated at a temperature of 350 °C to a pressure of  $4 \times 10^{-1}$  Pa. The specific surface area of the catalysts was determined according to BET at a relative partial pressure ( $p/p_0$ ) of 0.02. The pore size distribution was calculated by BJH method using the desorption curve. The total pore volume was determined according to BJH at  $p/p_0$  of 0.99. The Horvath-Kawazoe method was used to establish the specific surface area and volume of micropores.

*The acidic properties* of the samples were studied by the temperature-programmed desorption of ammonia ( $\text{NH}_3$ -TPD) on a USGA-101 universal sorption gas analyzer (Unisit, Russia). The weighed portion of the sample (0.15–0.20 g in the form of fraction 0.25–0.50 mm) was placed in a quartz reactor, heated in a flow of helium to a temperature of 500 °C at a ramp rate of 10 °C/min, calcined at this temperature for 1 h in a flow of helium, cooled to 60 °C, and saturated with ammonia in a flow of the dry mixture  $\text{NH}_3/\text{N}_2$  (1:1) for 15 min. To remove physically adsorbed ammonia the sample was held at 100 °C in a flow of dry helium for 1 h. The sample was then cooled to 60 °C in a flow of dry helium (feed velocity, 30 mL/min), and the reactor temperature was raised to 800 °C (at a ramp rate of 8 °C/min). The evolving ammonia was measured using a thermal conductivity detector.

X-ray absorption spectroscopy (XAS) was used to study *the local atomic environment* of Rh. EXAFS/XANES spectra of powdered samples (~100 mg) were taken at the “Structural Materials Science” beamline of the Kurchatov synchrotron radiation source [14,15]. Rh K-edge XAS spectra were measured in fluorescent mode, by means of Amptek X123 silicon drift detector (energy resolution ~100 eV). Si(220) channel-cut monochromator was used for energy scanning (energy resolution ~1 eV). The intensity of the monochromatic beam (both incident and transmitted) was measured with an ionization chamber filled with pure Ar. Primary processing of XAS spectra was carried out in terms of IFEFFIT software package [16,17]. Normalized EXAFS oscillations were  $k^3$ -weighted and analyzed in  $k$ -range of 2–12  $\text{\AA}^{-1}$ .

X-ray diffractometry (XRD) was used to study *the structure and phase composition of the samples*. X-ray diffraction patterns were taken at ‘X-ray Structural Analysis’ (XSA) beamline of Kurchatov synchrotron radiation source. The beam was monochromatized with a double-crystal Si (111) monochromator with a sagittally bent crystal focusing the beam to a size of 400  $\mu\text{m}$  in the horizontal plane. In the vertical plane, the beam was cut using collimator shutters, also to a size of 400  $\mu\text{m}$ . The radiation wavelength was 0.7200  $\text{\AA}$  with an energy resolution of  $\Delta E/E \sim 2 \times 10^{-4}$ .

Each sample was attached to a cryo-loop, which rotated 180° during the entire exposure time of 3 min. To record diffraction patterns, a two-dimensional MAR CCD detector was used, with a circular matrix of 160 mm in diameter and a pixel size of 79.7  $\mu\text{m}$ . The sample-to-detector distance was  $\sim 80$  mm and was refined (together with the angles of the detector tilts and instrumental broadening) in terms of Fit2d software [18] according to the diffraction pattern of the  $\text{Na}_2\text{Al}_2\text{Ca}_3\text{F}_{14}$  reference sample.

### 2.3. Catalytic activity tests

Experiments on the catalytic activity of the studied catalysts in the oxidative carbonylation of methane to AA were carried out in a 250 ml Teflon-coated stainless steel batch autoclave. A catalyst slurry in deionized water pretreated with ultrasound for 1 h was placed in the reactor. The catalyst slurry concentration was 1 wt %. The initial gas mixture consisting of methane (65.0 vol %), carbon monoxide (15.8 vol %), oxygen (4.0 vol %), and nitrogen (15.2 vol %) was injected into the reactor at room temperature at a pressure of 5.0 MPa. The following components were used for the preparation of gas mixtures: methane (99.99 vol %, TU 51-841-87), carbon monoxide (98 vol %, TU 6-02-7-101-86), compressed air (GOST 17433-80); all are manufactured by JSC “Moscow Gas Processing Plant”. The aqueous solution with dispersed catalyst particles was continuously and vigorously stirred by a mechanical stirrer at a speed of 650 rpm during the catalysis. The experiments were performed at a temperature of 150 °C and a pressure of 6.5 MPa. The reaction time was 24 h. The reaction temperature was measured through a thermocouple submerged to the water-catalyst slurry and monitored using a TRM-210 (LLC “OVEN production association”) automated temperature measuring/regulating controller. The catalytic test having been completed, the autoclave was cooled to 15 °C

with ice water bath. The dispersion medium with the reaction products was separated from the catalyst by centrifugation with a speed of 10,000 rpm using an AWTech TGL-16 M centrifuge (LLC “Labtech”). Each catalytic test was repeated at least three times.

The quantitative analysis of the products was determined by gas chromatography using Chrystallux 4000 (LLC “Metachrom production association”) instrument equipped chromatographic columns. A column packed with the activated carbon (1 m  $\times$  3 mm  $\times$  0.2–0.5 mm) was utilized to separate and analyze the gas products (except for oxygen). Oxygen was analyzed on a column packed with NaX zeolite (3 m  $\times$  3 mm  $\times$  0.18–0.25 mm). A Poraplot Q capillary column (25 m  $\times$  0.53 mm  $\times$  10  $\mu\text{m}$ ) was applied to determine the liquid products (oxygenates). The gas chromatography was performed in the programmed temperature rise mode from 50 to 280 °C with argon being carrier gas (50 ml/min). The amounts of gas and liquid components were estimated based on the integrated peak areas produced by a TCD and FID, respectively.

The chromatographic peaks were processed using NetChromWin software application.

The product yields were calculated according to Eq. (1):

$$\text{Yield} = \frac{n_{\text{product}}}{m_{\text{cat}}}, \cdot \mu\text{mol} \cdot \text{g}_{\text{cat}}^{-1} \quad (1)$$

where  $n_{\text{product}}$  and  $m_{\text{cat}}$  are amounts of product ( $\mu\text{mol}$ ) and catalyst weight (g), respectively.

## 3. Results and discussion

### 3.1. Physico-chemical properties of rhodium-containing catalysts based on microporous and micro-mesoporous zeolites

All the studied samples of Rh/HZSM-5, regardless of the zeolite

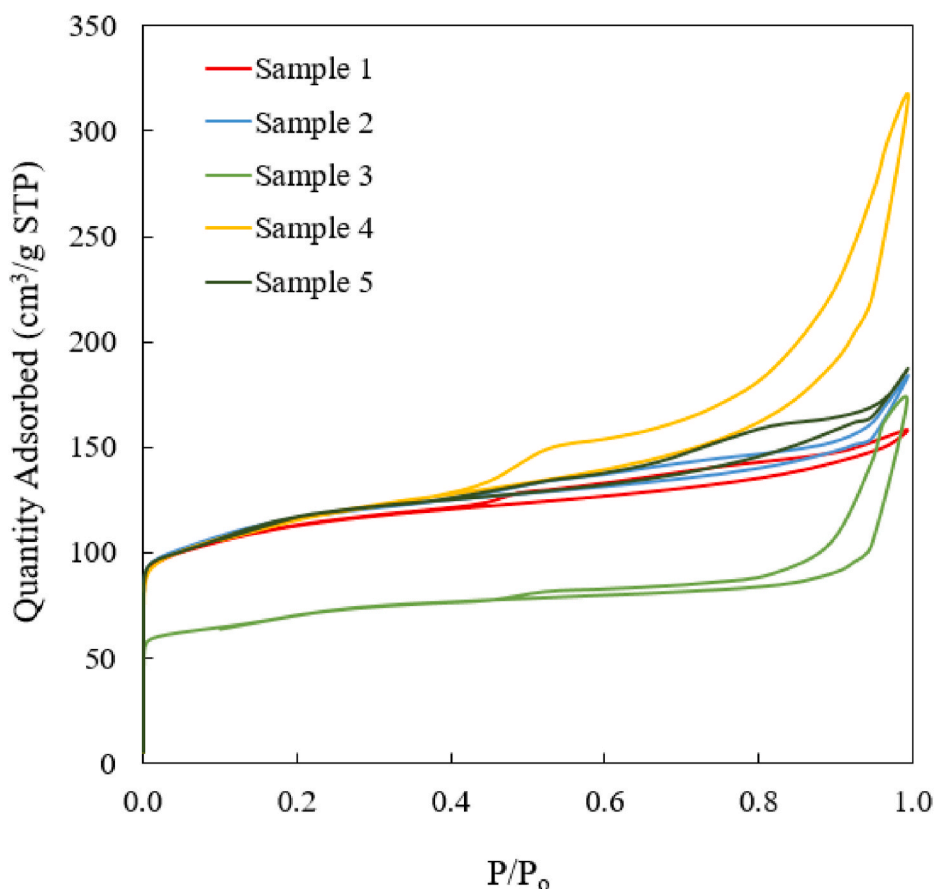


Fig. 1.  $\text{N}_2$  adsorption-desorption isotherms of the rhodium-containing catalysts based on microporous and micro-mesoporous zeolites.

pretreatment, are characterized by the typical zeolite isotherm (Fig. 1). The presence of a hysteresis loop indicates the occurrence of mesopores connecting with the environment through micropores.

Analysis of the porous structure parameters of the samples (Table 1) shows that post-synthetic treatment of HZSM-5 with both NaOH solution and ultrasound leads to an increase in its mesoporosity. The use of UST contributes to a growth the BET surface area ( $S_{\text{BET}}$ ) and the external surface area ( $S_{\text{ext}}$ ), and DS, in contrast, sharp decreases them. When combining UST and DS (samples 4 and 5),  $S_{\text{BET}}$  changes little, and  $S_{\text{ext}}$  much increases compared to sample 2 as UST is used only. At the same time, the total pore volume ( $V_{\text{total}}$ ) increases at the expense of the mesopore volume ( $V_{\text{meso}}$ ) with the micropore volume ( $V_{\text{micro}}$ ) decreasing slightly. The sequence of post-synthetic treatments is also of great importance. While processing the zeolite by the DS method followed by UST (sample 4),  $V_{\text{meso}}$  is almost twice as large as if exposed to UST with subsequent treatment by the DS method (sample 5),  $S_{\text{BET}}$  and  $V_{\text{micro}}$  are meanwhile not altered.

Post-synthetic treatment of the zeolites by the DS method considerable reduces the total acidity and increases the ratio of medium (I) acid sites to strong (II) acid sites (Fig. 2, Table 1). UST enhances the total acidity, I/II increases insignificantly. However, when UST and DS are combined (samples 4 and 5), I/II declines, while the total acidity decreases slightly and even increases in the case of zeolite treatment by the DS method followed by UST (sample 4). Therefore, desilication of zeolite enables an increase in the proportion of medium acid sites, and the combination of UST and DS, in contrast, increases the proportion of strong acid sites.

XAS method shows that depending on the history of the samples, the formation of various stabilization rhodium forms is possible (Fig. 3), and they are located mostly on the surface of the zeolite (the microstructural analyses of the catalysts is given in the Supplementary data (Fig. S3)). According to X-ray photoelectron spectroscopy data (Supplementary data, Fig. S4), the rhodium in the composition of the samples is present in the form of  $\text{Rh}_2\text{O}_3$  (the binding energy of the Rh  $3d_{5/2}$  sublevel 308.8 eV).

The shape of the spectra in the XANES region of the samples 2 and 5 is appropriate for platinumoid metals in zeolites and corresponds to an asymmetric or disordered oxygen environment. The spectra 3 and 4 are very different from 2 to 5, the absorption edge is shifted towards lower energies, which probably implies the rhodium reduction. On the EXAFS curve for samples 3 and 4, a maximum characteristic of metallic coordination is observed at  $R \sim 2.5 \text{ \AA}$ . For samples 2 and 5, there is a maximum at  $R \sim 1.5 \text{ \AA}$  indicating the oxygen coordination, but a weak maximum at  $R \sim 2.5 \text{ \AA}$  is also present, which may suggest either the reduction of a small fraction of rhodium or the formation of small clusters (dimers or trimers). EXAFS modeling results are given in the Supplementary data (Table S3).

X-ray diffraction analysis of the studied samples (Fig. 4) shows that the XRD patterns are identical for samples 2 and 5 with oxygen coordination of rhodium. For sample 3 with metallic rhodium coordination, an additional wide peak is present on the XRD pattern, which attributes to metal rhodium particles that most likely indicates the appearance of rhodium nanoclusters. Still, for sample 4, wherein the rhodium coordination, according to EXAFS data, is metallic as well, no such a peak is

observed. Nevertheless, the peaks assigned to the zeolite structure are expanded compared to the other samples. This may point to that the zeolite structure is disordered or deformed, apparently due to the formation of rhodium nanoclusters in the zeolite cavities invisible to XRD.

Hence, the EXAFS/XANES analysis reveals that in the samples pretreated with ultrasound, a single-center distribution of isolated  $\text{Rh}^+$  cations is mainly observed. In the samples initially treated using the DS method, rhodium nanoclusters are formed, and even the subsequent UST of such samples does not allow to the transition of rhodium to oxygen coordination. UST, in this case (sample 4), only “drives” the formed rhodium nanoclusters into the pores.

### 3.2. Catalytic activity of rhodium-containing catalysts based on microporous and micro-mesoporous zeolites

In order to evaluate the effect of the zeolite texture properties on the efficiency of catalysis in the oxidative carbonylation of methane to acetic acid, the catalytic activity of rhodium-containing catalysts based on microporous and micro-mesoporous zeolites was compared (Table 2). Error bars of the experimental data are given in the Supplementary data (Fig. S5).

Since methane is in a large excess as against to the other components of the reacting mixture, its conversion is slight and not exceeding 3%. Conversion of  $\text{O}_2$  and CO was 91 and 55%, respectively.

The microporous Rh/ZSM-5 zeolite catalyst (sample 1) under liquid-phase conditions exhibits a sufficiently high performance towards oxygenates, with the AA being formed almost twice as much as methanol. Pretreatment of zeolite with ultrasound (sample 2) increases the AA yield and decreases the methanol yield.

Pretreatment of zeolite with alkali (sample 3) leads to a markedly increase in the total yield of oxygenates, largely owing to methanol.

The joint UST and DS of the zeolites (samples 4 and 5) improves the yield of total oxygenates, mainly due to the AA formation, while the sequence of treatments is of great importance. Thus, when processing zeolite by the DS method followed by the UST (sample 4), the AA yield significantly increases and the methanol yield falls dramatically. At the same time, the UST of zeolite with subsequent treatment by the DS method promotes even greater increase in the AA yield and a decrease in the methanol yield.

Therefore the yield of oxygenates is greatly influenced by the textural, acidic properties of zeolite (Z), and the rhodium state in the catalyst. Methane activation can occur to form  $\text{Z-CH}_3$  both on the acid sites of the zeolite and on  $\text{Rh}^+$  cations giving  $\text{Rh-CH}_3$ . According to various reports [2,8,19,20], CO can be inserted directly into the  $\text{Rh-CH}_3$  bond in the presence of oxygen to form  $\text{Rh-CO-CH}_3$ . This insertion is supported by the zeolite acidity. Thus, acid sites on the zeolite surface play a crucial role in the oxidative conversion of methane to AA, and Rh present in the zeolite system enhances oxidative carbonylation of methane. Gain in AA yield after UST is most likely due to an increase in the acidity of the sample (sample 2, Table 1).

The increase in the yield of oxygenates, mainly through increased methanol yield, on sample 3 is due to the fact that during the processing of zeolite with alkali, first of all, aluminum atoms located in the intersectional cavities of the ZSM-5 lattice are “leached out”. The authors

**Table 1**

Texture properties and acidity and of the rhodium-containing catalysts based on microporous and micro- and mesoporous zeolites.

Sample	$S_{\text{BET}}, \text{m}^2 \cdot \text{g}^{-1}$	$S_{\text{micro}}, \text{m}^2 \cdot \text{g}^{-1}$	$S_{\text{ext}}, \text{m}^2 \cdot \text{g}^{-1}$	$V_{\text{total}}, \text{cm}^3 \cdot \text{g}^{-1}$	$V_{\text{micro}}, \text{cm}^3 \cdot \text{g}^{-1}$	$V_{\text{meso}}, \text{cm}^3 \cdot \text{g}^{-1}$	Density of acid sites, $\mu\text{mol} \cdot \text{g}^{-1}$			I/II <sup>a</sup>
							Total	I	II	
1	358.9	215.0	143.9	0.231	0.111	0.120	260	130	130	1.0
2	369.4	202.5	166.9	0.284	0.106	0.178	300	162	138	1.2
3	226.9	98.6	128.3	0.266	0.052	0.214	147	97	50	1.9
4	373.3	182.9	190.5	0.488	0.096	0.392	356	180	176	1.0
5	372.5	181.6	190.9	0.289	0.096	0.193	256	120	136	0.9

<sup>a</sup> The ratio of the proportion of acid sites of medium strength to strong acid sites.

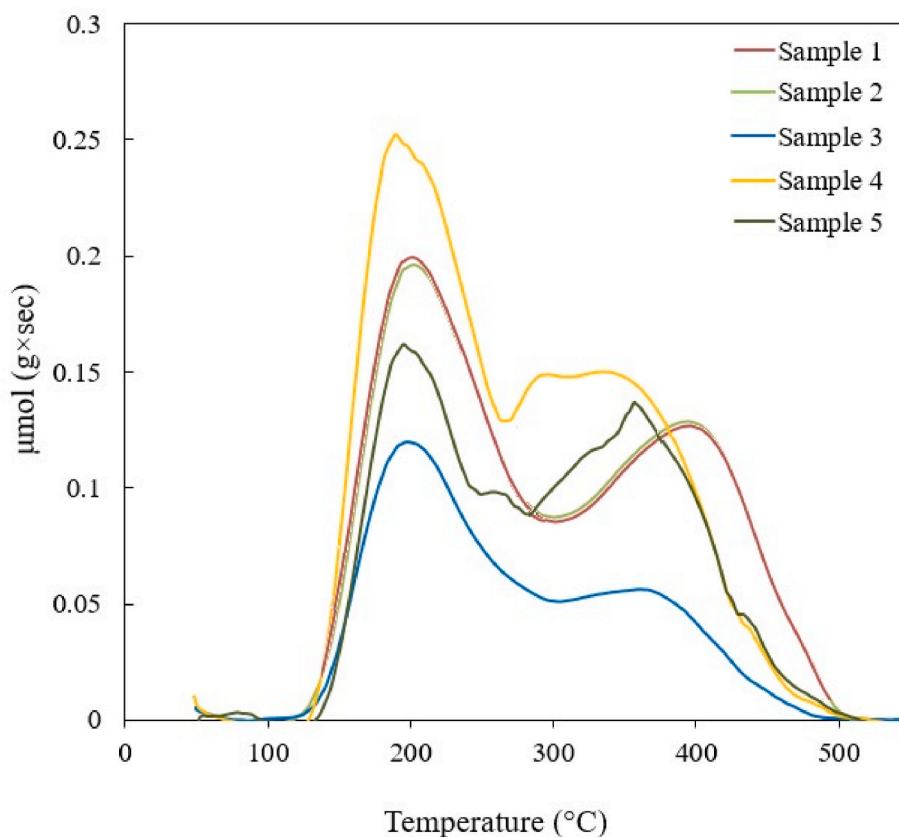


Fig. 2. NH<sub>3</sub>-TPD profiles of the rhodium-containing catalysts based on microporous and micro-mesoporous zeolites.

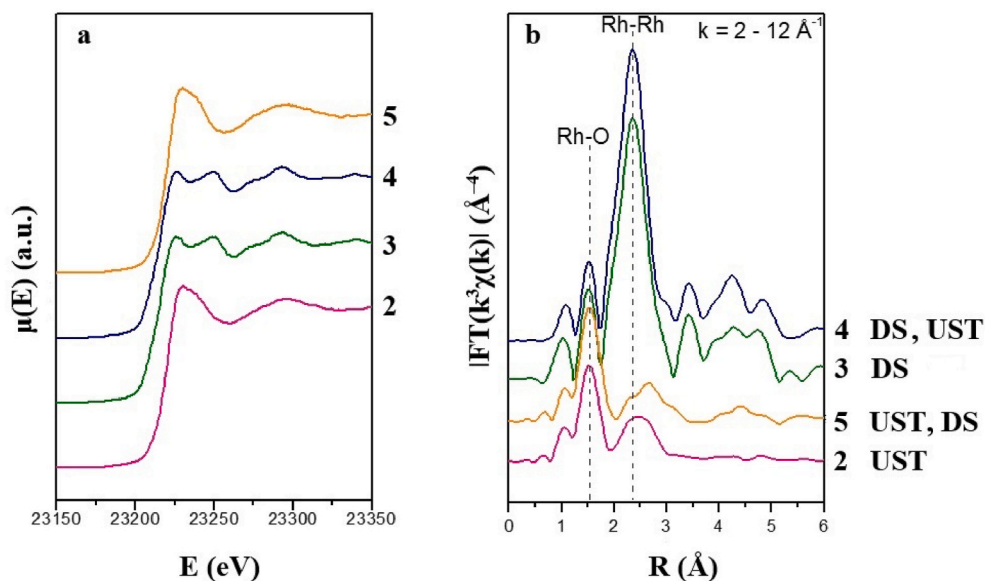


Fig. 3. XANES (a) and EXAFS (b) spectra of the rhodium-containing catalysts based on microporous and micro-mesoporous zeolites.

[21,22] calculated by the DFT method in combination with micro-kinetic analysis that the formation of acetyl products (methyl acetate and AA) occurs only in the direct channels of the MFI lattice, and acid sites localized in intersectional planes can induce the conversion of methanol into undesirable by-products resulting in a rapid deactivation of the HZSM-5 catalyst. The drop in the AA yield is explained by the rather low zeolite acidity. In addition, the formation of a developed mesopore system in zeolite decreases diffusion resistance, which reduces

the likelihood of secondary reactions, namely carbonylation of methanol into AA.

The change in catalytic properties during the joint processing of the parent zeolite (DS + UST) cannot be accounted only for the acidic and textural properties of the samples. Most likely, this is associated to the local environment of rhodium. As can be seen from the XAS data (Fig. 3), all samples contain isolated Rh<sup>+</sup> cations. Still, in addition to isolated Rh<sup>+</sup> cations, the formation of rhodium nanoclusters is observed on

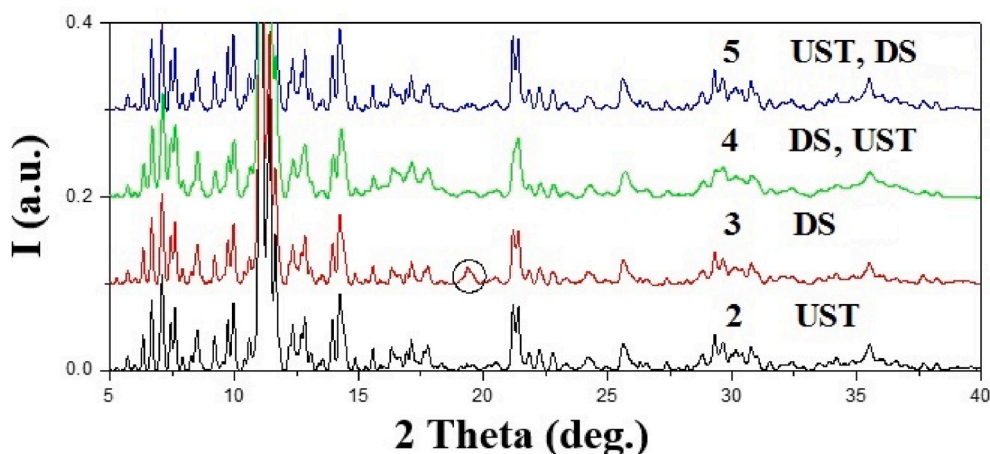


Fig. 4. XRD patterns of the rhodium-containing catalysts based on microporous and micro-mesoporous zeolites.

Table 2

Catalytic of rhodium-containing catalysts based on microporous and micro-mesoporous zeolites in the oxidative carbonylation of methane to acetic acid.

Sample	Zeolite treatment	Yield of products, $\mu\text{mol}\cdot\text{g}_{\text{cat}}^{-1}$			Methanol/AA, $\mu\text{mol}/\mu\text{mol}$
		Methanol	AA	Total	
1	Untreated	211	394	605	0.5
2	UST	100	450	550	0.2
3	DS	440	250	690	1.8
4	DS, UST	240	410	650	0.6
5	UST, DS	151	570	721	0.3

Conditions: initial gases consist of  $\text{CH}_4$  (65.0 vol %),  $\text{CO}$  (15.8 vol %),  $\text{O}_2$  (4.0 vol %), and  $\text{N}_2$  (15.2 vol %); catalyst slurry concentration is 1 wt %,  $T = 150^\circ\text{C}$ ,  $P = 6.5$  MPa, residence time is 24 h.

samples 3 and 4, while the treatment of zeolite by the DS method followed by UST (sample 4) according to the XRD (Fig. 4) “drives” the formed Rh nanoclusters into the pores. Thus, it can be assumed that methanol is predominantly formed on rhodium clusters, and AA formation is facilitated by a single-center distribution of isolated  $\text{Rh}^+$  cations, which is consistent with the literature data [23].

#### 4. Conclusions

In summary, it was first demonstrated that in liquid-phase conditions, an increase in the mesoporosity of ZSM-5 zeolite boosts the activity of a rhodium-containing catalyst in the oxidative carbonylation of methane to acetic acid (AA yield is  $570 \mu\text{mol}\cdot\text{g}_{\text{cat}}^{-1}$ ). To increase the mesoporosity of zeolite, two approaches were used: UST and DS of zeolite. Preliminary UST of the zeolite improves the AA yield with a decrease in the total yield of oxygenates. The methanol yield reduces as result of increase in the catalyst acidity, which promotes to the methanol carbonylation. DS of the zeolite leads to an increase in the total yield of oxygenates, mainly due to methanol; a decrease in the AA yield is associated with the low acidity and the formation of a developed mesopore system in the zeolite, which slows down secondary reactions (methanol carbonylation). The combination of these two factors declines in the AA yield. The combined use of UST and DS of the zeolite allows to increase the total yield of oxygenates while improving the AA yield. Such a change in the catalytic properties is attributable to both the acidity of the parent zeolite and the local environment of rhodium. XAS analysis showed that rhodium on the zeolite surface can be present either as nanoclusters producing methanol or as isolated rhodium atoms intensifying the AA formation.

#### CRediT authorship contribution statement

**Natalia V. Kolesnichenko:** Conceptualization, Methodology, Supervision, Writing – original draft, Writing – review & editing. **Yulia M. Snatenkova:** Resources, Investigation. **Tatiana I. Batova:** Writing – original draft, Writing – review & editing. **Olga V. Yashina:** Investigation, Formal analysis, Validation. **Konstantin B. Golubev:** Writing – original draft.

#### Declaration of competing interest

The authors declare that they have no known competing financial interests or personal relationships that could have appeared to influence the work reported in this paper.

#### Acknowledgements

This work was supported by the Russian Science Foundation (Project No. 21-73-20042). This work was performed using the equipment of the Shared Research Center «Analytical center of deep oil processing and petrochemistry of TIPS RAS».

The authors are grateful to Ph.D. EV Khramov (National Research Center “Kurchatov Institute”) for carrying out studies by the XAS spectroscopy method and for help in discussing the results.

#### Appendix A. Supplementary data

Supplementary data to this article can be found online at <https://doi.org/10.1016/j.micromeso.2021.111581>.

#### References

- [1] R. Periana, D. Taube, S. Gamble, Platinum catalysts for the high-yield oxidation of methane to a methanol derivative, *Science* 280 (1998) 560–564, <https://doi.org/10.1126/science.280.5363.560>.
- [2] R. Periana, O. Mironov, D. Taube, Catalytic, oxidative condensation of  $\text{CH}_4$  to  $\text{CH}_3\text{COOH}$  in one step via CH activation, *Science* 301 (2003) 814–818, <https://doi.org/10.1126/science.1086466>.
- [3] A. Kokalj, N. Bonini, C. Sbraccia, Engineering the reactivity of metal catalysts: a model study of methane dehydrogenation on Rh (111), *J. Am. Chem. Soc.* 126 (2004) 16732–16733, <https://doi.org/10.1021/ja045169h>.
- [4] J. Shan, M. Li, L. Allard, S. Lee, M. Flytzani-Stephanopoulos, Mild oxidation of methane to methanol or acetic acid on supported isolated rhodium catalysts, *Nature* 551 (2017) 605–608, <https://doi.org/10.1038/nature24640>.
- [5] T. Moteki, N. Tominaga, M. Ogura, CO-assisted direct methane conversion into  $\text{C}_1$  and  $\text{C}_2$  oxygenates over ZSM-5 supported transition and platinum group metal catalysts using oxygen as an oxidant, *ChemCatChem* 12 (2020) 2957–2961, <https://doi.org/10.1002/cctc.202000168>.
- [6] K.B. Golubev, O.V. Yashina, T.I. Batova, N.V. Kolesnichenko, N.N. Ezhova, Direct low-temperature oxidative conversion of methane to acetic acid over rhodium-

- modified zeolites, *Petrol. Chem.* 61 (2021) 663–669, <https://doi.org/10.1134/S0965544121040058>.
- [7] Y. Tang, Y. Li, V. Fung, D. Jiang, W. Huang, Sh Zhang, Y. Iwasawa, T. Sakata, L. Nguyen, X. Zhang, A. Frenkel, F. Tao, Single rhodium atoms anchored in micropores for efficient transformation of methane under mild conditions, *Nat. Commun.* 9 (2018) 1231–1242, <https://doi.org/10.1038/s41467-018-03235-7>.
- [8] J. Shan, M. Li, L. Allard, S. Lee, M. Flytzani-Stephanopoulos, Mild oxidation of methane to methanol or acetic acid on supported isolated rhodium catalysts, *Nature* 551 (2017) 605–608, <https://doi.org/10.1038/nature24640>.
- [9] K. Tarach, K. Góra-Marek, J. Martínez-Triguero, I. Melián-Cabrer, Acidity and accessibility studies of desilicated ZSM-5 zeolites in terms of their effectiveness as catalysts in acid-catalyzed cracking processes, *Catal. Sci. Technol.* 7 (2017) 858–873, <https://doi.org/10.1039/C6CY02609E>.
- [10] N. Kolesnichenko, O. Yashina, N. Ezhova, G. Bondarenko, S. Khadzhiev, Nanodispersed suspensions of zeolite catalysts for converting dimethyl ether into olefins, *Russ. J. Phys. Chem. A* 92 (2018) 118–123, <https://doi.org/10.1134/S0036024418010120>.
- [11] S. Mitchell, A. Pinar, J. Kenvin, P. Crivelli, J. Kärger, J. Pérez-Ramírez, Structural analysis of hierarchically organized zeolites, *Nat. Commun.* 6 (2015) 8633, <https://doi.org/10.1038/ncomms9633>.
- [12] J. Groen, W. Zhu, S. Brouwer, S. Huynink, F. Kapteijn, J. Moulijn, Direct demonstration of enhanced diffusion in mesoporous ZSM-5 zeolite obtained via controlled desilication, *J. Am. Chem. Soc.* 129 (2007) 355–360, <https://doi.org/10.1021/ja065737o>.
- [13] J. Groen, T. Bach, U. Ziese, A. Paulaime-van Donk, K. de Jong, J. Moulijn, Creation of hollow zeolite architectures by controlled desilication of Al-zoned ZSM-5 crystals, *J. Am. Chem. Soc.* 127 (2005) 10792–10793, <https://doi.org/10.1021/ja052592x>.
- [14] A. Chernyshov, A. Veligzhanin, Y. Zubavichus, Structural materials science end-station at the Kurchatov synchrotron radiation source: recent instrumentation upgrades and experimental results, *Nucl. Instrum. Methods Phys. Res. A* 603 (2009) 95–98, <https://doi.org/10.1016/j.nima.2008.12.167>.
- [15] N. Trofimova, A. Veligzhanin, V. Murzin, A. Chernyshov, E. Khramov, V. Zabluda, I. Edel'man, Y. Slovokhotov, Y. Zubavichus, Structural diagnostics of functional nanomaterials with the use of X-ray synchrotron radiation, *Russ. Nanotechnol.* 8 (2013) 396–401, <https://doi.org/10.1134/S1995078013030191>.
- [16] B. Ravel, M. Newville, ATHENA, artemis, HEPHAESTUS: data analysis for X-ray absorption spectroscopy using IFEFFIT, *J. Synchrotron Radiat.* 12 (2005) 537–541, <https://doi.org/10.1107/S0909049505012719>.
- [17] M. Newville, IFEFFIT: interactive XAFS analysis and FEFF fitting, *J. Synchrotron Radiat.* 8 (2001) 322–324, <https://doi.org/10.1107/s0909049500016964>.
- [18] A. Hammersley, FIT2D: an Introduction and Overview, *ESRF Internal Report*, 1997. ESRF97HA02T.
- [19] X. Wang, et al., NMR-spectroscopic evidence of intermediate-dependent pathways for acetic acid formation from methane and carbon monoxide over a ZnZSM-5 zeolite catalyst, *Angew. Chem. Int. Ed.* 51 (2012) 3850–3853, <https://doi.org/10.1002/anie.201108634>.
- [20] K.J. Cavell, Recent fundamental studies on migratory insertion into metal-carbon bonds, *Coord. Chem. Rev.* 155 (1996) 209–243, [https://doi.org/10.1016/S0010-8545\(96\)90182-4](https://doi.org/10.1016/S0010-8545(96)90182-4).
- [21] A.K. Md, L. Rahman, M. Kumashiro, T. Ishihara, Direct synthesis of formic acid by partial oxidation of methane on H-ZSM-5 solid acid catalyst, *Catal. Commun.* 12 (2011) 1198–1200, <https://doi.org/10.1016/j.catcom.2011.04.001>.
- [22] S. Wang, S. Guo, Y. Luo, Z. Qin, Y. Chen, M. Dong, J. Li, W. Fan, J. Wang, Direct synthesis of acetic acid from carbon dioxide and methane over Cu-modulated BEA, MFI, MOR and TON zeolites: a density functional theory study, *Cat. Sci. Tech.* 9 (2019) 6613–6626, <https://doi.org/10.1039/c9cy01803d>.
- [23] D. Kim, A. Kim, T. Chang, H. Koo, J. Kim, G. Han, C. Shin, J. Bae, Synergy effects of Al<sub>2</sub>O<sub>3</sub> promoter on a highly ordered mesoporous heterogeneous Rh-g-C<sub>3</sub>N<sub>4</sub> for a liquid-phase carbonylation of methanol, *Appl. Catal., A: GEN* 585 (2019) 117209, <https://doi.org/10.1016/j.apcata.2019.117209>.